Mn^{III}ImH, 79969-69-0; (TPP)$Mn^{III}(ImH)_2Cl$, 100082-46-0; TPP(Cl)-Mn^{III}*N*-MeIm, 79969-71-4; (TPP)Mn^{III}(*N*-MeIm)$_2$Cl, 100082-48-2; TPP(Cl)Mn^{III}3,4-Py, 100082-47-1; (TPP)$Mn^{III}(3,4\text{-Py})_2Cl$, 100082-49-3; TPP(Cl)$Mn^{III}$NAcPhIm, 100082-50-6; TPP(Cl)Mn^{III}2,6-Py, 100082-51-7; (TPP)$Mn^{III}Cl$, 32195-55-4; $Ph_2C(CN)OOH$, 5233-67-0; $(CH_3)_3$-COOH, 75-91-2; *p*-NO_2-Ph-CO_3H, 943-39-5; $PhCH_2CO_3H$, 19910-09-9; $CH_3(CH_2)_{10}CO_3H$, 2388-12-7; $Ph_2C(CO_2Me)OOH$, 57272-44-3; PhC-$(CH_3)_2OOH$, 80-15-9.

High- and Low-Potential Flavin Mimics. 3. 3,7,10-Trimethyl-(1*H*,3*H*,5*H*,7*H*,9*H*,10*H*)-pyrimido[5,4-*g*]pteridine-2,4,6,8-tetrone-Mediated Reduction of Carbon–Carbon Double Bonds α–β to an Acyl Function

Edward B. Skibo*† and Thomas C. Bruice*‡

Contribution from the Department of Chemistry, Arizona State University, Tempe, Arizona 85287, and the Department of Chemistry, University of California at Santa Barbara, Santa Barbara, California 93106. *Received August 15, 1985*

Abstract: The reduction of the carbon–carbon double bond of maleimide (MI), *N*-methylmaleimide (NMM), ethyl fumarate, diethyl fumarate, diethyl maleate, fumaric acid, and maleic acid was investigated by employing the low redox potential flavin mimic 3,7,10-trimethyl-(1*H*,3*H*,5*H*,7*H*,9*H*,10*H*)-pyrimido[5,4-*g*]pteridine-2,4,6,8-tetrone ($PPTH_2$) as the reductant. The reaction of these substrates with $PPTH_2$ to produce PPT_{ox} and the corresponding succinimide or succinate consists of three processes. The first process occurs on mixing and pertains to the formation of a mixture of N(1)- and C(4a)-substrate adducts of $PPTH_2$. The other two processes, which are kinetically distinguishable, pertain to the breakdown of each of these adducts to PPT_{ox} and the reduced substrate. Breakdown of the C(4a)-adduct is catalyzed by hydroxide and is independent of substrate concentration. Hydroxide catalysis is proposed to represent a concerted process whereby the hydroxide abstracts the N(5)-proton while the anionic reduced substrate is departing (Brønsted β approaching 1.0). Breakdown of the N(1)-adduct to the observed products is substrate-dependent pertaining to the rate-determining formation of the N(9),C(4a)-diadduct. In a fast step, base-catalyzed elimination from the C(4a)-position of the latter provides the reduced substrate anion and the N(9)-monosubstrate adduct of PPT_{ox}. Rapid dissociation of the N(9)-adduct then provides PPT_{ox}. It is concluded that the reduction of a carbon–carbon double bond to an acyl function by the low-potential flavin mimic proceeds via C(4a)-adducts. This conclusion and the principle of microreversibility infers that enzyme-bound flavins of high potential, as in dehydrogenating flavoenzymes, may oxidize succinates to fumarates via C(4a)-adducts.

Model studies have provided insights into the mechanisms of the diverse redox reactions mediated by flavoenzymes.[1] As a model for these reactions, the lumiflavin redox couple (Fl_{ox}/FlH^-), or a suitable analogue thereof, is employed as an oxidant or reductant of the substrate in an enzyme-free reaction. Results

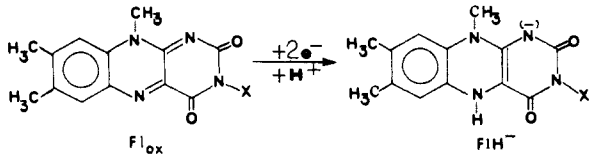

(1)

of such studies have served to provide a chemical basis upon which flavoenzyme mechanisms may rest. Flavoenzymes involved in oxidative formation and retroreduction of C–C double bonds α, β to a carbonyl group have been studied in this fashion. By employing FlH^- as the reductant for *N*-methylmaleimide (NMM) and maleimide (MI), Venkataram and Bruice[2] determined that electron transfer occurs via the C(4a)-adduct, eq 2.

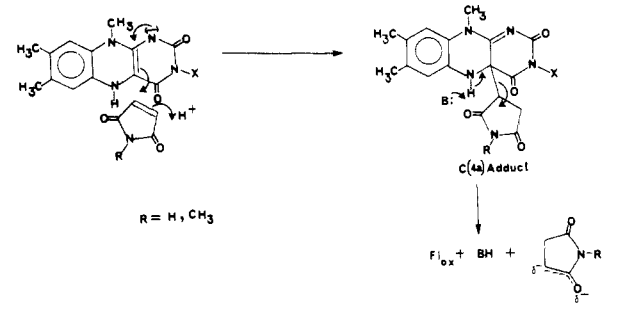

(2)

It was concluded by these workers that succinic acid dehydrogenase and fumarate reductase[3] may likewise transfer electrons via a similar adduct. The conclusion regarding succinic acid dehydrogenase invokes the principle of microreversibility which states that the transition state for the forward process (reduction of NMM and MI) is the same as that for the reverse process (oxidation of the corresponding succinimides). The principle of microreversibility must be used in conjunction with the model approach since the redox potential of the enzyme-bound flavin is difficult to match with a mimic. Indeed the redox potentials of flavoenzymes may be far removed from that of the free cofactor in aqueous buffer (Fl_{ox}/FlH^-, $E^{\circ\prime} = -0.189$ V). Notable examples are glucose oxidase[4] (two-electron potential, $E^{\circ\prime} = 0.0$ V) and thiamine dehydrogenase[5] (single-electron potentials of $E_1^{\circ\cdot} = +0.08$ V and $E_2^{\circ\cdot} = +0.03$ V). The reduction potential of

† Arizona State University.
‡ University of California at Santa Barbara.

(1) (a) Bruice, T. C. *Acc. Chem. Res.* **1980**, *13*, 256. (b) Bruice, T. C. In "Biomimetic Chemistry"; Dolphin, D., McKenna, C., Murakami, Y., Tabushi, I., Eds.; Wiley: New York, 1980; ACS Adv. Chem. Ser. No. 191, p 89.
(2) Venkataram, U. V.; Bruice, T. C. *J. Am. Chem. Soc.* **1984**, *106*, 5703.
(3) Walsh, C. *Acc. Chem. Res.* **1980**, *13*, 148.
(4) Stankovich, M. T.; Schopfer, L. M.; Massey, V. *J. Biol. Chem.* **1978**, *253*, 4971.
(5) Edmondson, D. E.; Gomez-Moreno, C. In "Flavins and Flavoproteins"; Yagi, K., Yamano, T., Eds.; University Park Press: Baltimore, 1980; p 297.

0002-7863/86/1508-1650$01.50/0

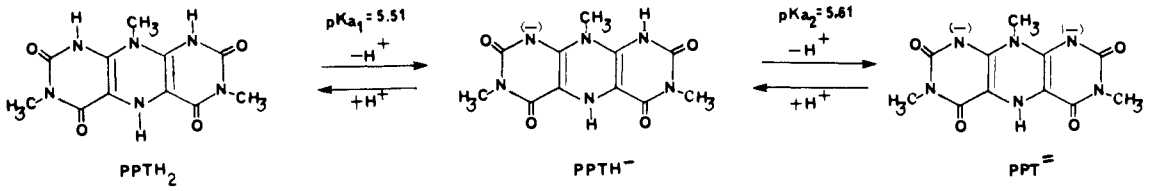

(4)

Fl_{ox}/FlH^- is not sufficiently low to allow the facile reduction of maleates or fumarates ($E^{\circ\prime}$ = 0.031 V)[6] to the corresponding succinates. The oxidative reactions of interest may be studied by examining the mechanism of the retroreductive process with a low potential flavin mimic. Such a mimic has been realized in the pyrimido[5,4-*g*]pteridine redox couple[7] found in eq 3.

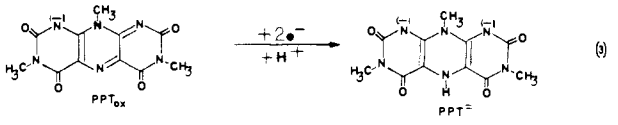

(3)

On the basis of comparative studies of the PPT^{2-}- and FlH^--mediated reduction of formaldehyde, the couple PPT_{ox}/PPT^{2-} ($E^{\circ\prime}$ = −0.346 V) acts as a low reduction potential flavin mimic.[7b] This powerful organic reducing agent has been shown to be capable of reducing fumarates and maleates[7a] as well as disulfide bonds.[7b] Even the reduction of an aromatic aldehyde to the hydrocarbon was facilitated by two two-electron transfers from PPT^{2-} in aqueous buffer.

The objective of this study has been to investigate in detail the reduction of NMM, MI, diethyl fumarate, diethyl maleate, and the corresponding carboxylic acids by PPT^{2-}. We show herein that reduction of these substrates occurs via C(4a)-adducts. This result strongly suggests that high potential flavoenzymes oxidize succinate to fumarate via a C(4a)-adduct.

Experimental Section

Instruments. All kinetic mechanisms were carried out on either a Cary 118 spectrometer or Perkin-Elmer Lambda-3 spectrometer in which the cell holder had been maintained at 30.0 ± 0.2 °C by circulating thermostated water. pH measurements were carried out on a Radiometer Model M26 pH meter equipped with a Radiometer GK2402C glass–calomel combination electrode. GC analyses were carried out on a Varian 3700 series gas chromatograph (5% OV-17 on Chromosorb 80-100W-HP, 6-ft column) using a Varian CDS101 electronic integrator for peak determinations.

Materials. *N*-Methylmaleimide was obtained from Sigma Chemical Co. and maleimide was obtained from Aldrich Chemical Co. GC analyses indicated that both compounds were sufficiently pure to use as such. *N*-Methylsuccinimide was prepared by the catalytic hydrogenation of *N*-methylmaleimide: mp 64 °C [lit.[8] 66 °C]. 3,7,10-Trimethyl-(1*H*,3*H*,7*H*,10*H*)-pyrimido[5,4-*g*]pteridine-2,4,6,8-tetrone (PPT_{ox}) was prepared as previously described.[7c] The inorganic salts used in the preparation of buffer solutions were of analytical reagent grade obtained from Mallinkrodt and were used as such. The buffer solutions were prepared by using doubly glass distilled water. The ionic strength of all buffers was adjusted to 1.0 with KCl.

Kinetic Measurements. Reduction of *N*-methylmaleimide, maleimide, diethyl fumarate, ethyl fumarate, and diethyl maleate by $PPTH_{2T}$ were followed in Thunberg cuvettes at 30.0 ± 0.2 °C under an argon atmosphere. The following buffer systems were used to maintain pH: formic acid/formate, pK_a = 3.75; acetic acid/acetate, pK_a = 4.55; phosphate monobasic/phosphate dibasic, pK_a = 6.50; and carbonate monobasic/carbonate dibasic, pK_a = 9.66. These buffer pK_a values were obtained in aqueous buffer at 30 °C with μ = 1.0 (KCl). Details of the preparation of similar kinetic runs are described in an earlier report.[7b] Stock solutions of *N*-methylmaleimide and maleimide for these studies were always prepared at the time of the run. At pH 7.00 or above, stock solutions were made with 1 M KCl. Otherwise, the stock solutions were prepared with the buffer employed to hold the pH of the kinetic run. For kinetic studies of the reduction of diethyl fumarate, ethyl fumarate, and diethyl maleate, stock solutions were prepared with Me_2SO. The resulting reaction mixtures consisted of 10% Me_2SO or less.

Preparative Study of *N*-Methylmaleimide (NMM) Reduction by $PPTH_{2T}$. The preparation of solid $PPTH_2$ was carried out as previously described.[7b] To a reaction mixture consisting of 6.9 g (0.023 mol) of $PPTH_2$ suspended in 200 mL of water under a strict anaerobic atmosphere there was added 2.0 g (0.0177 mol) of *N*-methylmaleimide. The reaction mixture was then stirred for 4 days, maintaining the anaerobic atmosphere.

The reaction was then removed to the air and extracted 5 times with 20-mL portions of $CHCl_3$. The *N*-methylsuccinimide, 0.5 g (24%), and unreacted *N*-methylmaleimide, 1.1 g (56%), were assayed by GC employing standards prepared with authentic *N*-methylsuccinimide and *N*-methylmaleimide. Verification of the identity as *N*-methylsuccinimide was made by isolation: The $CHCl_3$ extracts were washed with pH 7.0 phosphate buffer containing 10% cysteine to remove unreacted *N*-methylmaleimide. Drying of the chloroform layer ($MgSO_4$) and concentration provided a solid residue. Double sublimation yielded pure *N*-methylsuccimide identified as such by a mixed melting point and ^1H NMR.

Preparative Study of Diethyl Fumarate Reduction by $PPTH_{2T}$. To a solution consisting of 1.0 g (5.8 mmol) of diethyl fumarate in 40 mL of DMF and 115 mL of 0.33 M pH 7.0 phosphate buffer there was added 1.70 g (5.8 mmol) of $PPTH_2$. The reaction was stirred for 12 h under strict anaerobic conditions. After the reaction was removed to the air and diluted to 250 mL with H_2O, extraction was carried out with 3 × 150 mL portions of chloroform followed by drying ($MgSO_4$) of the extracts. Diethyl succinate, 0.32 g (32%), was assayed by GC employing authentic diethyl succinate as a standard. Verification of the identity as diethyl succinate was made by concentration of the $CHCl_3$ extracts to an oil; IR and ^1H NMR spectra of this oil were seen to be identical with authentic material.

The isolation and identification of hydrolysis products were carried out as follows. The pH 7.0 aqueous fractions previously extracted with chloroform were placed on a 100 mL AG 1 × 2, 200–400 mesh Cl^- column (Bio Rad). The column was washed with 500 mL of distilled water and then 250 mL of 0.01 M HCl with which UV absorbing products were eluded. TLC [*n*-butanol, acetic acid, water (5:2:3)] on silica gel indicated that only ethyl fumarate and fumaric acid were present. Yields of 0.07 g (10%) of fumaric acid and 0.16 g (19%) of ethyl fumarate were estimated by ^1H NMR.

Results

The reductions of *N*-methylmaleimide (NMM) and maleimide (MI) by $PPTH_{2T}$ (=$PPTH_2$ + $PPTH^-$ + PPT^{2-}) were studied under anaerobic conditions in aqueous buffer (μ = 1.0, KCl) at 30.0 ± 0.2 °C by using the pseudo-first-order conditions of [NMM] and [MI] ≫ [$PPTH_{2T}$] = 1 × 10^{-5} M. Reactions proceeded to >90% completion as evidenced by the final absorbance of PPT_{ox} at 423 nm. A preparative study of the reduction of NMM by $PPTH_{2T}$ in aqueous solvent verified that *N*-methylsuccinimide was the reduction product; see Experimental Section.

***N*-Methylmaleimide Reduction by $PPTH_{2T}$.** The reduction of NMM by $PPTH_{2T}$ was studied in the pH range of 2–10.7 with [NMM] = 8.6 × 10^{-2} to 1.9 × 10^{-4} M. Repetitive scanning of reaction solutions, each initially containing pseudo-first-order concentrations of NMM and 1.0 × 10^{-5} M $PPTH_{2T}$ at various pH values, from 700 to 350 nm revealed that the buildup of PPT_{ox} (423 nm) was not associated with the formation of any absorbing intermediate(s) (repetitive scans not shown).

Plots of the absorbance of PPT_{ox} (423 nm) vs. time obtained below pH 7.5 could be fit to a two consecutive first-order rate law (eq 5). Found in Figure 1 are examples of these plots obtained from the reaction of 1.0 × 10^{-5} M $PPTH_{2T}$ with various concentrations of NMM in anaerobic 1.0 M pH 5.50 acetate buffer.

$$OD_{423} = A \exp(-k_{obsd}t) + B \exp(-k'_{obsd}t) + C \quad (5)$$

(6) Burton, T. *Ergeb. Physiol.* **1957**, *49*, 275.

(7) (a) Skibo, E. B.; Bruice, T. C. *J. Am. Chem. Soc.* **1982**, *104*, 4982. (b) Skibo, E. B.; Bruice, T. C. *Ibid.* **1983**, *105*, 3316. (c) Skibo, E. B.; Bruice, T. C. *Ibid.* **1983**, *105*, 3304.

(8) "Handbook of Chemistry and Physics", 60th ed.; Weast, R. C., Ed.; CRC Press: Cleveland, 1980.

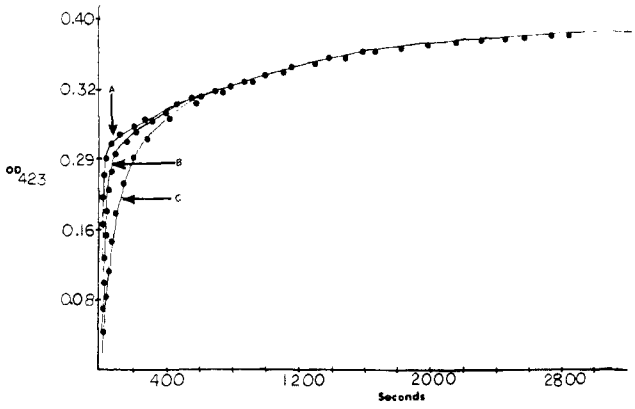

Figure 1. Absorbance (423 nm) vs. time (s) plots for the reduction of NMM by 1×10^{-5} M $PPTH_{2T}$ in 1.0 M pH 5.50 acetate buffer, μ = 1.0 KCl, at 30 °C under argon. [NMM] = 1.67×10^{-2} M (A), 8.39×10^{-3} M (B), and 4.19×10^{-3} M (C).

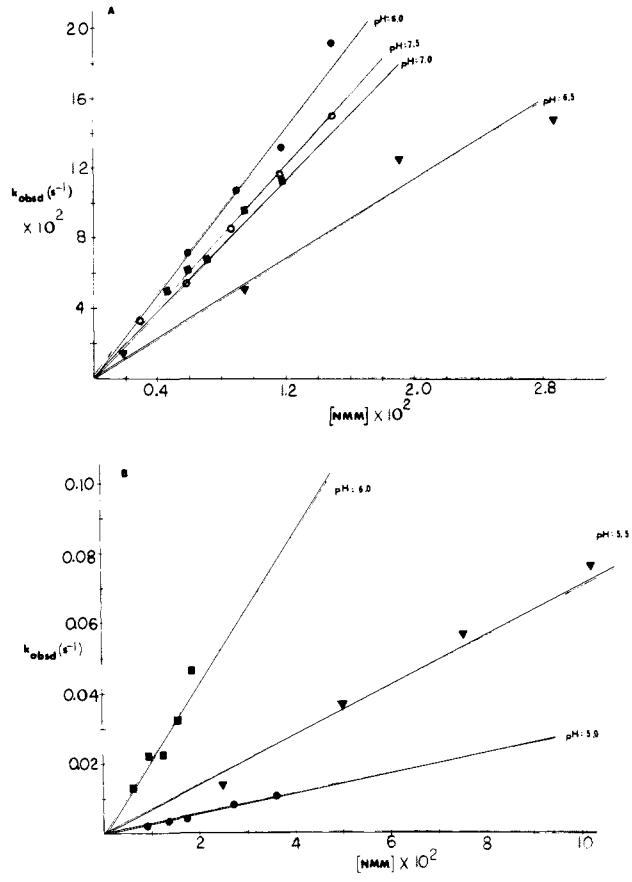

Figure 2. Plots of k_{obsd} (s^{-1}) vs. [NMM] for the first phase of PPT_{ox} formation employing 1.0×10^{-5} M $PPTH_{2T}$ in the following anaerobic buffers. A: (●) 0.8 M, pH 9.00 carbonate buffer; (○) 0.3 M, pH 7.5 phosphate buffer; (■) 0.26 M, pH 7.0 phosphate buffer; (▼) 0.3 M, pH 6.5 phosphate buffer. B: (●) 1 M, pH 5.00 acetate buffer; (▼) 1 M, pH 5.50 acetate buffer; and (■) 0.75 M, pH 6.0 acetate buffer.

In eq 5, k_{obsd} and k'_{obsd} are pseudo-first-order rate constants, A/B represents the ratio of $[PPT_{ox}]$ produced during the first phase to $[PPT_{ox}]$ produced during the second phase, and C is the absorbance at t_∞ (0.4 M^{-1} cm^{-1} for 1×10^{-5} M PPT_{ox}). As is apparent from Figure 1, the first phase of PPT_{ox} formation (k_{obsd} in eq 5) is dependent on [NMM] and the second slower phase of PPT_{ox} formation (k'_{obsd} in eq 5) is not. Thus, plots of k_{obsd} vs. [NMM] are linear with a zero intercept and provide as slopes the pH-dependent second-order rate constant for PPT_{ox} formation (k, M^{-1} s^{-1}) during the first phase, Figures 2 and 3. Plots of k'_{obsd} vs. [NMM] (not shown) were found to be of zero slope showing the lack of dependence of the second phase on substrate concentration. Above pH 7.5, the formation of PPT_{ox} follows a

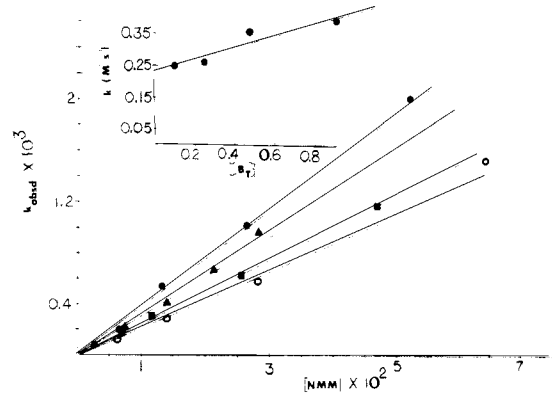

Figure 3. Plots of k_{obsd} (s^{-1}) vs. [NMM] in anaerobic pH 4.00 acetate buffer at various values of $[B_T]$: (●) $[B_T]$ = 0.92; (▲) $[B_T]$ = 0.47; (■) $[B_T]$ = 0.24; (○) $[B_T]$ = 0.092. The inset is a plot of the slopes (k, M^{-1} s^{-1}) vs. $[B_T]$.

first-order rate law and the values of k_{obsd} are linearly dependent upon [NMM], Figure 2. Thus, above pH 7.5, the second phase of PPT_{ox} formation (k'_{obsd}) is of no importance. To assess the pH dependence of k_{obsd} under very basic conditions, its value was determined at pH 10.7 in 0.2 M carbonate buffer. Much above pH 9.0, the hydrolysis of NMM is significant and must be corrected for. In a separate experiment NMM hydrolysis in 0.2 M pH 10.7 carbonate buffer was observed to occur at 0.123 s^{-1}. Simulation of the increase in PPT_{ox} absorbance with time employing computer fitting with eq 6 provided the value of 125 M^{-1} s^{-1} for k_{obsd} at pH 10.7 (where NMS is *N*-methylsuccinimide).

$$\text{NMM} + \text{PPTH}_{2T} \xrightarrow{k_{obsd}} \text{NMS} + \text{PPT}_{ox}$$

$$\text{NMM} \xrightarrow{k_{hyd} = 0.123\ s^{-1}} \text{hydrolysis products} \qquad (6)$$

To assess the role of buffers in PPT_{ox} formation, buffer dilution studies were carried out at the constant acidities of pH 3.0 (formate), pH 4.0 (acetate), pH 6.0 (acetate), and pH 7.0 (phosphate). The second-order rate constant for PPT_{ox} formation during the first phase (k, M^{-1} s^{-1}) exhibited buffer catalysis only at pH 3.0 and 4.0, while the pseudo-first-order rate constant for PPT_{ox} formation during the second phase (k'_{obsd}) did not exhibit buffer catalysis at any pH value (Table I, Figure 3). Extrapolation of the buffer-dependent values of k(M^{-1} s^{-1}) to zero buffer (Figure 3) provided as the intercept the buffer-independent apparent second-order rate constant (k_{lyate}). The ratio of $[PPT_{ox}]$ formed during the first phase to that formed during the second phase (A/B) was also found to be dependent on buffer concentration. Average values of A/B were plotted against $[Buffer_T]$ at the constant acidities of pH 3.0, 4.0, 6.0, and 7.0 (Figure 4). These plots indicate that A/B is very dependent on $[B_T]$ at the pH values of 6.0 and 7.0 but much less so at the pH values of 3.0 and 4.0.

The plot of the log of the buffer-independent second-order rate constants (k_{lyate}) for PPT_{ox} formation during the first phase vs. pH is found in Figure 5A. The solid line of Figure 5A was computer-generated from eq 7 by using $\bar{k}$ = 125 M^{-1} s^{-1} and pK_{a1} = 6.65. The plot of the log of the pseudo-first-order rate constant (k'_{obsd}) for PPT_{ox} formation during the second phase vs. pH is found in Figure 5B. The solid line of Figure 5B was computer-generated from eq 8 by using $\bar{\bar{k}} = 9.35 \times 10^{-8}$ s^{-1}, $k_{HO^-} = 3.14 \times 10^4$ M^{-1} s^{-1}, pK_a = 3.96, and pK_w = 13.83.

$$k_{lyate} = \frac{\bar{k}K_{a1}}{K_{a1} + a_H} \qquad (7)$$

$$k'_{obsd} = \frac{\bar{\bar{k}}}{K_a + a_H} + \frac{k_{HO^-}K_w}{a_H} \qquad (8)$$

Maleimide Reduction by $PPTH_{2T}$. The reduction of maleimide (MI) to succinimide by $PPTH_{2T}$ was studied in the pH range of 2–7.50 under the pseudo-first-order conditions of [MI] = 1.33×10^{-4} to 1.2×10^{-2} M $\gg$ $[PPTH_{2T}] = 1 \times 10^{-5}$ M. Many aspects

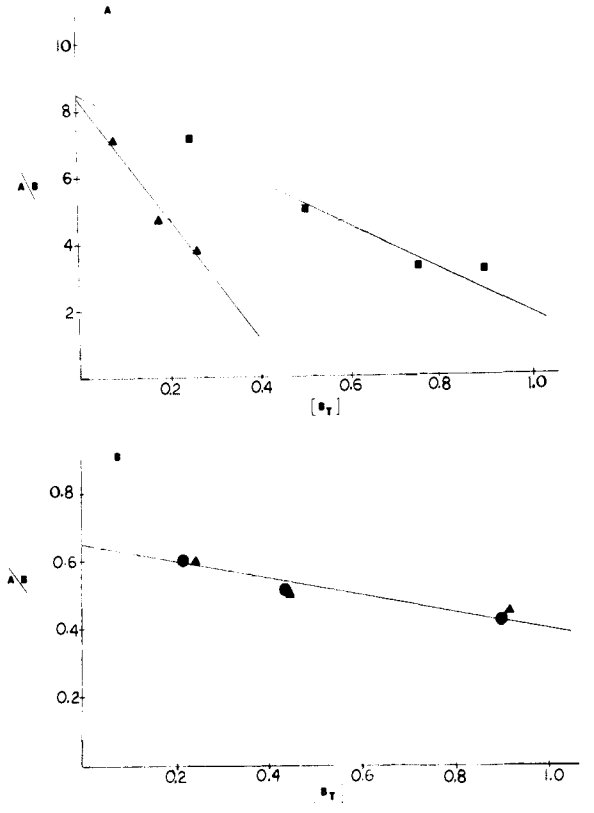

Figure 4. Plots of A/B values determined from eq 5 vs. total buffer concentration ($[B_T]$). Each A/B value is the average of five determinations at constant pH and $[B_T]$ under anaerobic conditions. A: (■) pH 7.0 phosphate buffer; (▲) pH 6.0 acetate buffer. B: (●) pH 4.0 acetate buffer; (▲) pH 3.0 formate buffer.

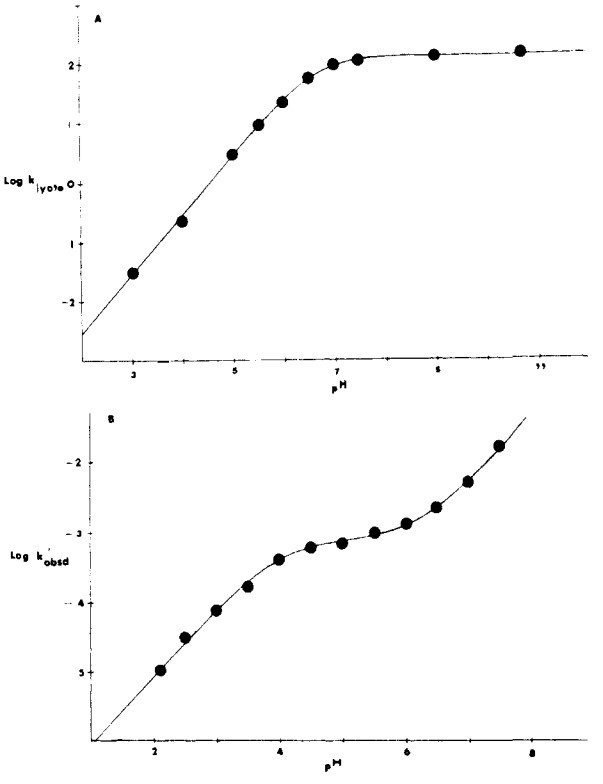

Figure 5. (A) Plot of log k_{lyate} vs. pH for the first phase of NMM reduction by 1×10^{-5} M $PPTH_{2T}$ in anaerobic buffer at 30 °C. (B) Plot of log k'_{obsd} vs. pH for the second phase of NMM reduction by 1×10^{-5} M $PPTH_{2T}$ in anaerobic buffer at 30 °C.

of maleimide reduction by $PPTH_{2T}$ parallel those found in the *N*-methylmaleimide reduction study. Thus, reactions followed

Table I. Values of k_{obsd} and k'_{obsd} Obtained from the Reaction of *N*-Methylmaleimide (NMM) with 1×10^{-5} M $PPTH_2T$ at Various Values of $[B_T]$ at the pH Values of 3.00, 6.00, and 7.00 (μ = 1.0 with KCl at 30 °C under Anaerobic Conditions)

10^2[NMM]	$[B_T]$	10^3k_{obsd}, s^{-1}	$10^5k'_{obsd}$, s^{-1}
	In pH 3.00 Formate Buffer		
6.08	0.92	4.08	9.0
7.6	0.92	5.82	8.0
4.0	0.92	2.38	7.8
3.0	0.92	1.89	7.24
2.0	0.92	1.35	7.6
1.5	0.92	1.00	7.7
1.0	0.92	0.66	7.7
2.73	0.47	1.22	7.03
2.05	0.47	0.91	7.08
1.37	0.47	0.49	6.7
0.68	0.47	0.32	7.66
2.72	0.24	1.08	7.1
2.04	0.24	0.63	6.4
1.45	0.24	0.53	7.8
0.68	0.24	0.24	8.3
2.80	0.092	0.84	7.36
2.10	0.092	0.7	7.88
1.4	0.092	0.32	7.8
10^3[NMM]	$[B_T]$	10^2k_{obsd}, s^{-1}	$10^3k'_{obsd}$, s^{-1}
	In pH 6.00 Buffer		
2.20	0.90	5.13	1.39
1.83	0.90	4.34	1.33
1.46	0.90	2.86	1.41
1.10	0.90	2.58	1.62
0.73	0.90	1.58	1.29
1.89	0.75	4.65	1.30
1.58	0.75	3.24	1.40
1.26	0.75	2.23	1.35
0.95	0.75	2.23	1.28
0.63	0.75	1.31	1.28
2.16	0.50	4.56	1.02
1.80	0.50	3.91	1.37
1.44	0.50	2.48	1.67
1.08	0.50	2.28	1.41
0.72	0.50	1.52	1.34
2.32	0.25	5.86	1.3
1.93	0.25	4.90	1.4
1.54	0.25	3.56	1.28
1.15	0.25	2.6	1.5
0.77	0.25	1.6	1.5
10^{-4}[NMM]	$[B_T]$	10^2k_{obsd}, s^{-1}	$10^3k'_{obsd}$, s^{-1}
	In pH 7.00 Buffer		
11.76	0.264	11.2	4.96
9.41	0.264	9.60	4.94
7.06	0.264	6.77	5.13
5.88	0.264	6.22	5.18
4.70	0.264	4.95	5.61
2.35	0.264	2.21	6.01
12.26	0.264	12.17	4.56
10.22	0.178	9.06	4.47
8.17	0.178	7.92	4.70
6.13	0.178	5.37	4.30
4.09	0.178	3.54	4.98
10.77	0.082	9.42	4.77
8.97	0.082	8.33	5.33
7.18	0.082	6.22	5.31
5.38	0.082	4.61	5.02
3.59	0.082	2.59	4.88

at 423 nm exhibited PPT_{ox} formation to >90% completion. Below pH 7.5, absorbance (423 nm) vs. time (seconds) plots for PPT_{ox} formation were two consecutive first order in nature and could be fit to eq 5. As in the case of NMM reduction, PPT_{ox} formation occurs by a substrate-dependent phase (k_{obsd}) and by a slower substrate-independent phase (k'_{obsd}). Much above pH 7.5, only the substrate-dependent phase was apparent.

To assess the nature of substrate dependence of the first phase of PPT_{ox} formation, plots of k_{obsd} vs. [MI] were made at all pH values studied. Below pH 5.0, these plots displayed saturation in [MI] with slopes approaching zero at high values of [MI] (not

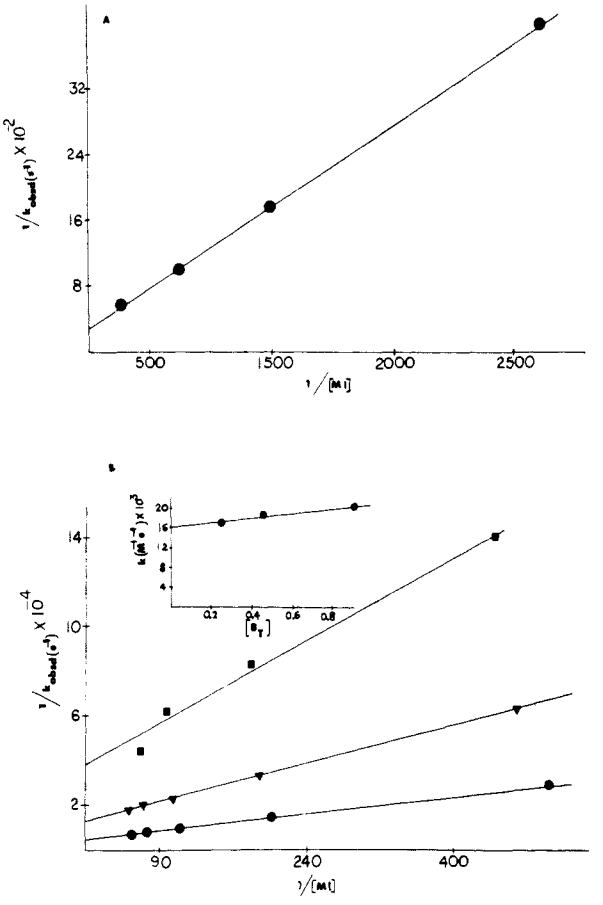

Figure 6. (A) Plot of $1/k_{obsd}$ (s^{-1}) vs. 1/[MI] for the first phase of PPT_{ox} formation determined in anaerobic 1 M, pH 5.00 acetate buffer. (B) Plots of $1/k_{obsd}$ (s^{-1}) vs. 1/[MI] for the first phase of PPT_{ox} formation obtained under anaerobic conditions in various buffers: (■) 1 M, pH 2.00 formate; (▼) 1 M, pH 2.50 formate; (●) 1 M, pH 3.00 formate. Inset is a plot of k (M^{-1} s^{-1}) vs. $[B_T]$ for pH 3.00 formate buffer.

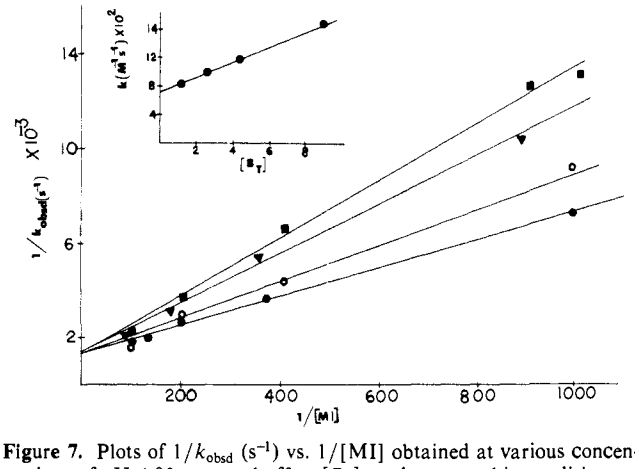

Figure 7. Plots of $1/k_{obsd}$ (s^{-1}) vs. 1/[MI] obtained at various concentrations of pH 4.00 acetate buffer, $[B_T]$, under anaerobic conditions at 30 °C: (●) $[B_T]$ = 0.9; (○) $[B_T]$ = 0.45; (▼) $[B_T]$ = 0.246; (■) $[B_T]$ = 0.09. Inset is a plot of k (M^{-1} s^{-1}) obtained from the reciprocal slopes vs. $[B_T]$.

shown). This observation suggests that the relationship between k_{obsd} and [MI] can be expressed by eq 9 where k is an apparent

$$k_{obsd} = \frac{k[MI]}{1 + K[MI]} \qquad (9)$$

second-order rate constant and K is an apparent equilibrium constant for the formation of an adduct of MI with the reducing species. Found in Figures 6 and 7 are reciprocal plots ($1/k_{obsd}$ vs. 1/[MI]) which provide the apparent second-order rate constant

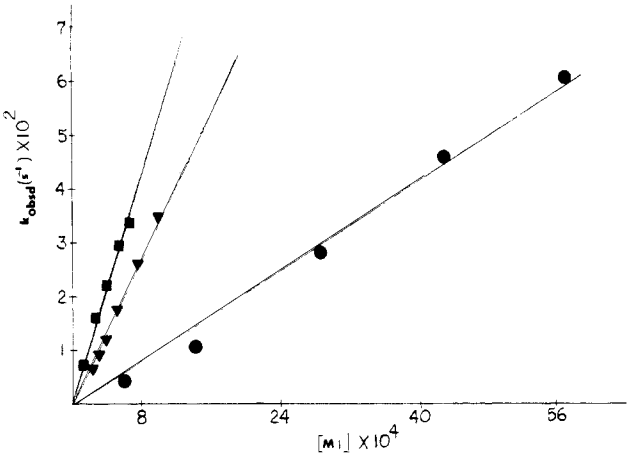

Figure 8. Plots of k_{obsd} (s^{-1}) vs. [MI] obtained in various anaerobic buffers: (●) 1 M, pH 6.00 acetate; (▼) 0.3 M, pH 7.0 phosphate; (■) 0.3 M, pH 7.50 phosphate.

(k, M^{-1} s^{-1}) as the reciprocal of the slope and the ratio K/k as the intercept. Much above pH 5.0, plots of k_{obsd} vs. [MI] were linear over the range of [MI] studied, Figure 8. The absence of saturation at pH values > 5.0 may be a consequence of K[MI] ≪ 1 in eq 9 at these acidities, resulting in $k_{obsd} = k$[MI]. The plots in Figure 8 thus provide as the slope the apparent second-order rate constant k(M^{-1} s^{-1}). Plots of k'_{obsd} vs. [MI] (not shown) were found to be of zero slope, showing the lack of dependence of the second phase on substrate concentration.

To assess the role of buffers in PPT_{ox} formation, buffer dilution studies were carried out at the constant acidities of pH 3.0 (formate), pH 4.0 (acetate), pH 6.0 (acetate), and pH 7.0 (phosphate). The apparent second-order rate constant for PPT_{ox} formation during the first phase (k, M^{-1} s^{-1}) was observed to be dependent on $[B_T]$ at pH 4.0 and 3.0. Found as insets in Figures 6B and 7 are plots of k (M^{-1} s^{-1}) vs. B_T at these acidities which provided as the intercept the buffer-independent values of the apparent second-order rate constant (k_{lyate}). At the lower constant acidities studied, pH 6.0 and 7.0, k was observed to be independent of $[B_T]$. At all acidities studied, the pseudo-first-order rate constants (k'_{obsd}) for PPT_{ox} formation during the second phase were independent of $[B_T]$.

Found in Figure 9A is a plot of the log of the buffer-independent second-order rate constants (k_{lyate}) for PPT_{ox} formation during the first phase vs. pH. The solid line was generated from eq 7 by using $\bar{k}$ = 58.5 M^{-1} s^{-1} and K_{a1} = 6.72. Found in Figure 9B is a plot of the log of the first-order rate constants (k'_{obsd}) for PPT_{ox} formation during the second phase vs. pH. The solid line was generated from eq 8 by using $\bar{k}$ = 2.5 × 10^{-7} s^{-1}, pK_a = 3.37, k_{HO^-} = 1.92 × 10^6 M^{-1} s^{-1}, and pK_w = 13.83.

Reduction of Fumaric and Maleic Acids Derivatives by $PPTH_{2T}$. Fumaric and maleic acid reductions by $PPTH_{2T}$ were studied in anaerobic pH 7.00 and 4.00 buffers by employing the pseudo-first-order conditions of 0.02–0.45 M substrate ≫ 1 × 10^{-5} M $PPTH_{2T}$. These reactions were quite slow, and only initial rates of PPT_{ox} formation were determined. For example, the reaction of 0.05 M fumaric acid with 1 × 10^{-5} M $PPTH_{2T}$ in pH 7.00 buffer provided PPT_{ox} at 1.4 × 10^{-6} OD_{432} s^{-1}. To assess the presence of oxygen-stable products in these reaction mixtures, aeration was carried out and the reoxidation to PPT_{ox} followed. Whereas reaction mixtures held at pH 7.00 rapidly re-formed PPT_{ox} to 100% yield upon aeration, those held at pH 4.00 did so by a slow zero-order process to afford a ≤100% yield of PPT_{ox}. For example, the zero-order formation of PPT_{ox} upon aeration of a reaction 0.09 M in fumarate buffer was measured as 3.5 × 10^{-3} OD_{423} s^{-1}. The percentage yield of PPT_{ox} upon aeration of the reaction mixtures was found to decrease with an increase of substrate concentration and the time allowed for incubation of reaction solutions prior to aeration. Thus, a reaction initially containing 0.02 M maleic acid and 1 × 10^{-5} M $PPTH_{2T}$ in 0.4 M acetate buffer rapidly formed PPT_{ox} to 100% upon addition

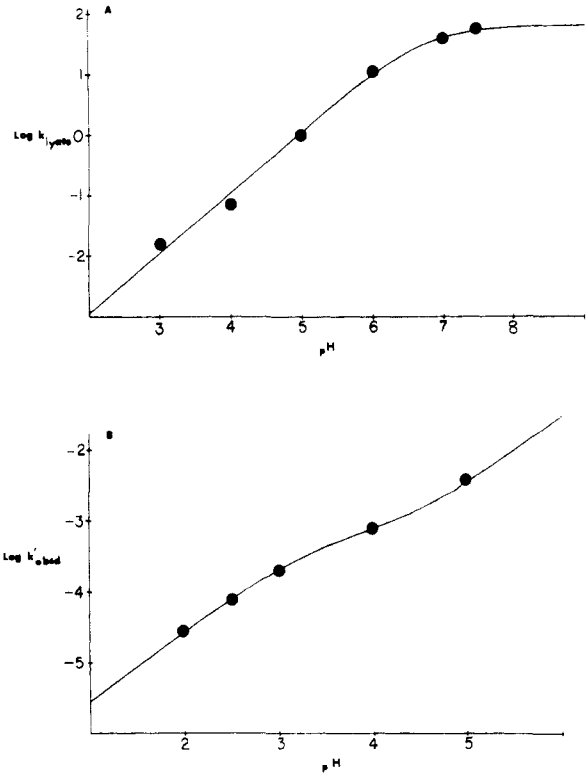

Figure 9. (A) Plot of log k_{lyate} vs. pH for the first phase of MI reduction by 1×10^{-5} M $PPTH_{2T}$ in anaerobic buffer at 30 °C. (B) Plot of log k'_{obsd} vs. pH for the second phase of MI reduction by 1×10^{-5} M $PPTH_{2T}$ in anaerobic buffer at 30 °C.

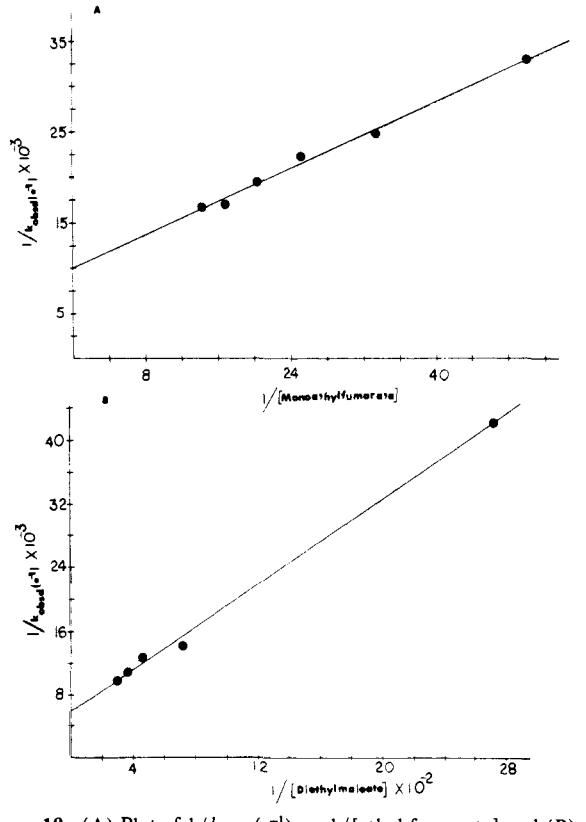

Figure 10. (A) Plot of $1/k_{obsd}$ (s^{-1}) vs. 1/[ethyl fumarate] and (B) plot of $1/k_{obsd}$ (s^{-1}) vs. 1/[diethyl maleate]. All reductions were carried out under pseudo-first-order conditions in anaerobic 0.33 M, pH 7.00 phosphate buffer at 30 °C.

of air after an incubation time of 2900 s. On the other hand, reactions initially containing 0.45 M maleic acid provided only 45% and 14% of the expected amount of PPT_{ox} upon addition of air after incubation times of 1×10^4 and 2×10^4 s, respectively. The reaction of 0.09 M fumarate buffer at pH 4.00 with 1×10^{-5} M $PPTH_{2T}$ provided 41% of the total expected PPT_{ox} upon addition of air after a 1.1×10^4 s incubation time.

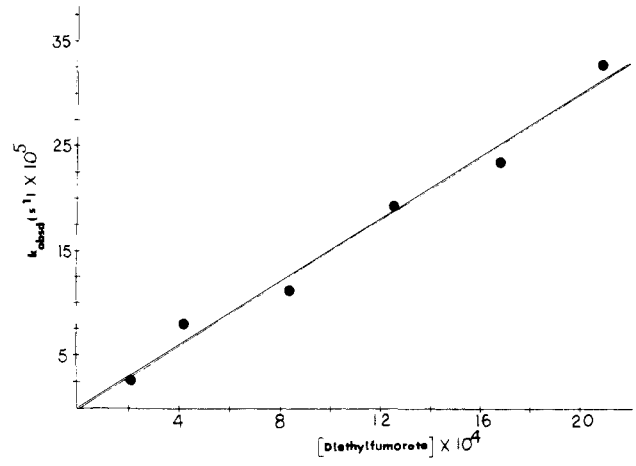

Figure 11. Plot of k_{obsd} (s^{-1}) vs. [diethyl fumarate] obtained under pseudo-first-order conditions in anaerobic 0.33 M, pH 7.00 phosphate buffer at 30 °C.

Reductions of diethyl fumarate, its half ester, and diethyl maleate by $PPTH_{2T}$ were studied in 0.33 M phosphate buffer at pH 7.00 and at 30 °C. Unlike the corresponding diacids, all reactions exhibited a first-order increase in PPT_{ox} to 75–100% completion. Saturation of rates on the increase of [substrate] in the cases of diethyl maleate and ethyl fumarate would be in accord with adduct formation on or off the reaction path. A plot of $1/k_{obsd}$ vs. 1/[ethyl fumarate] for the reduction of ethyl fumarate by $PPTH_{2T}$ (1×10^{-5} M) in pH 7.00 phosphate buffer gave a straight line with 1/slope = 2.2×10^{-3} M^{-1} s^{-1} and 1/intercept = 1×10^{-4} s^{-1} (Figure 10A). A plot of $1/k_{obsd}$ vs. 1/[diethyl maleate] provided 1/slope = 7.4×10^{-2} M^{-1} s^{-1} and 1/intercept = 2.37×10^{-3} s^{-1}, Figure 10B. A plot of k_{obsd} vs. [diethyl fumarate] for the reduction of diethyl fumarate by $PPTH_{2T}$ (1×10^{-5} M) passes through zero, providing the second-order rate, 0.15 M^{-1} s^{-1}, as the slope, Figure 11. For verification of succinates as the products of these reductions, diethyl fumarate (1.0 g, 5.8 mmol) was preparatively reduced by $PPTH_{2T}$ (1.7 g, 5.8 mmol) in DMF/pH 7.00 buffer (35:65) over a 4-day period (see Experimental Section). Diethyl succinate (54%) was the only reduction product and was accompanied by the hydrolytic products of diethyl fumarate which are ethyl fumarate (19%) and fumaric acid (10%).

Discussion

Formation of C(4a)- and N(1)-Adducts. Both *N*-methylmaleimide (NMM) and maleimide (MI) are proposed to form C(4a)- and N(1)-adducts with $PPTH_{2T}$ (=$PPTH_2$ + $PPTH^-$ + PPT^{2-}) on mixing, eq 10. Attempts to monitor the formation

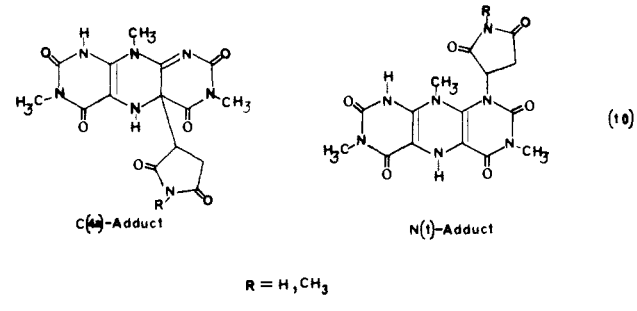

(10)

of adducts by stopped-flow spectrophotometry (320–360 nm) were frustrated by the very small changes in absorbance. The biphasic formation of PPT_{ox} pertains to the rate-determining decomposition of these adducts by different pH–rate laws and substrate dependencies. The first substrate-dependent and the second substrate-independent phases of PPT_{ox} formation are attributed to the breakdown of the N(1)- and C(4a)-adducts, respectively

Scheme I

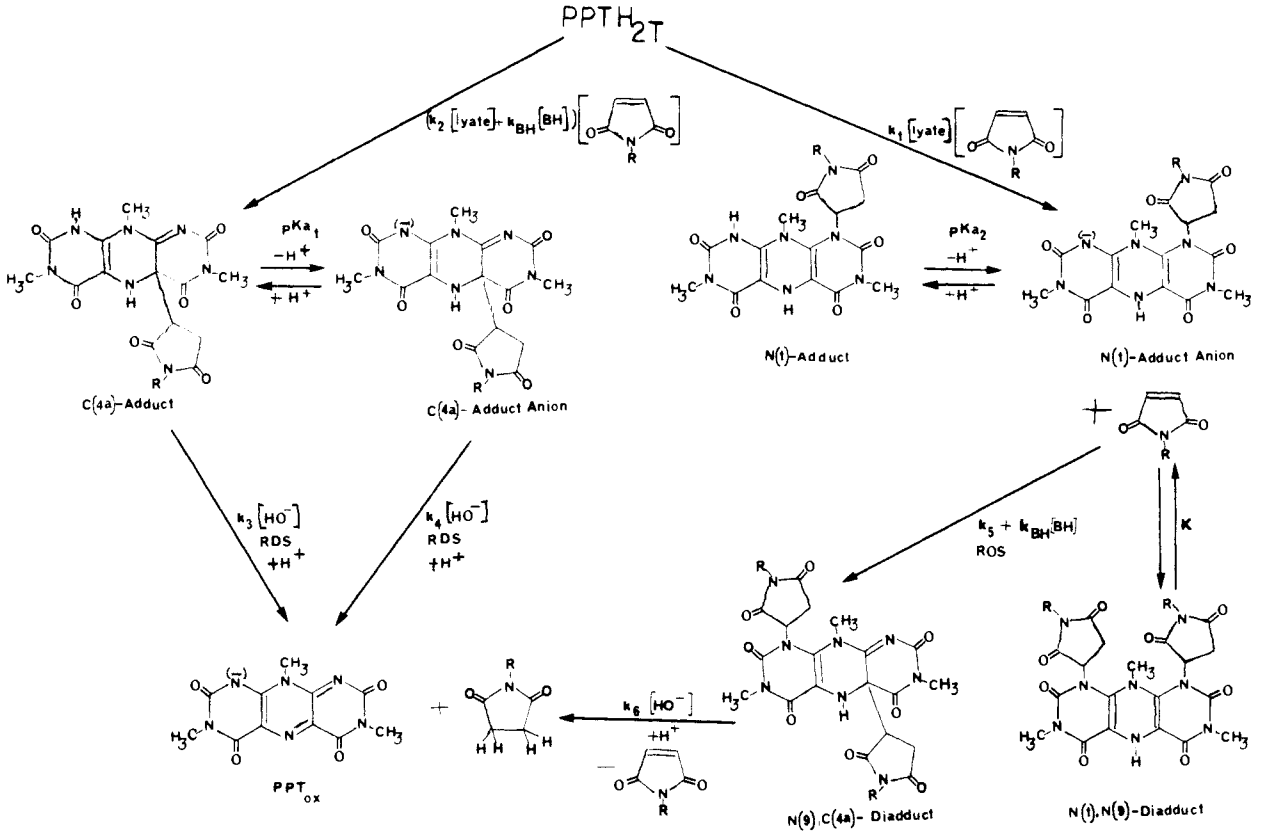

(Scheme I). In what follows is a discussion of the results of studies of NMM and MI reduction of $PPTH_{2T}$ which led to the assessments concerning adduct formation and structure.

That $PPTH_{2T}$ is not involved in the rate-determining step for PPT_{ox} formation is shown by the pH–rate profiles for PPT_{ox} formation. The pH–rate profiles for the first phase of PPT_{ox} formation obtained with NMM and MI as the substrates obeyed the single pK_a rate law found in eq 7 (loc. cit., Figures 5A and 9A). The apparent pK_a values obtained by fitting these profiles to eq 7 are 6.65 and 6.72 for NMM and MI, respectively. Similarly, the pH–rate profiles for the second phase of PPT_{ox} formation obtained with both substrates obeyed the single pK_a rate law found in eq 8 (loc. cit., Figures 5B and 9B). The apparent pK_a values obtained by fitting these profiles to eq 8 are 3.96 and 3.37 for NMM and MI, respectively. From these results, it is seen that the species which form PPT_{ox} in the rate-determining steps have one less acid dissociation than $PPTH_{2T}$ (loc. cit., eq 4). Furthermore, the apparent pK_a values cited above are significantly different from those for acid dissociation of $PPTH_2$, $pK_{a1} = 5.51$ and $pK_{a2} = 5.61$ in eq 4. The observed differences between the kinetically determined pK_a values and pK_{a1} and pK_{a2} for $PPTH_2$ could perhaps be explained by the presence of an equilibrium, in addition to acid dissociations, involving one of the forms of $PPTH_{2T}$. As Bruice and Schmir[9] pointed out, the constant for such an equilibrium will become part of the kinetically determined pK_a values. Consideration of the presence of an equilibrium involving one of the forms of $PPTH_{2T}$ (=$PPTH_2$ + $PPTH^-$ + PPT^{2-}) occurring before the rate-determining step provides pH–rate laws wherein one or both apparent pK_a values differ from pK_{a1} and pK_{a2}. There is no means, however, to justify a single pK_a for a reaction involving $PPTH_{2T}$ itself. A reasonable explanation for a single kinetic pK_a is found in the formation of adducts of $PPTH_2$ with NMM and MI which possess only one acid dissociation and which form PPT_{ox} in rate-determining steps. It has been documented that 1,5-dihydroflavin (FlH_2) reacts with NMM and MI to form C(4a)-adducts at stopped-flow rates.[2] The greater nucleophilicity of $PPTH_{2T}$ compared to 1,5-dihydroflavin has also been documented.[7] Thus, it is reasonable to postulate that $PPTH_{2T}$ forms adducts with NMM and MI on mixing. The only monoadducts of NMM and MI with $PPTH_{2T}$ possessing a single acid dissociation are the N(1)- and C(4a)-adducts shown in eq 10.

The ratio of [N(1)-adduct] to [C(4a)-adduct] formed on mixing NMM and MI with $PPTH_{2T}$ is given by A/B in eq 5 where A = [PPT_{ox}] formed from the N(1)-adduct during the first phase and B = [PPT_{ox}] formed from the C(4a)-adduct during the second phase. The bases for assigning the second phase of PPT_{ox} formation as C(4a)-adduct breakdown are as follows: (1) the rate law for the second phase and (2) the dependence of A/B on the total buffer concentration. In their study of NMM and MI reduction by FlH_2, Venkataram and Bruice[2] observed that the C(4a)-adduct of these substrates decomposes to Fl_{ox} by a rate law which is independent of substrate and first-order in hydroxide. Similarly, the second phase of PPT_{ox} formation is independent of substrate and obeys an analogous pH–rate law (vide infra). The above workers also investigated the mechanism of C(4a)-adduct formation; the general acid-catalyzed transfer of the substrate to the C(4a)-position of the N(1)-anion of FlH_2 was postulated. Likewise, we postulate this mechanism for C(4a)-adduct formation from PPT^{2-}, **1**.

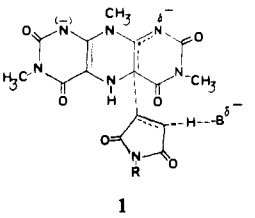

1

Evidence of buffer catalysis is seen in the changes in A/B with 10-fold changes in the buffer at the constant acidities of pH 7.00, 6.00, 4.00, and 3.00 (loc. cit., Figure 4). At the constant acidities of pH 6.00 and 7.00, the A/B ratio decreases significantly with the total buffer concentration even though the observed rate constants are independent of the buffer. At the higher acidities of pH 3.00 and 4.00, the A/B ratio likewise decreases with the

(9) Bruice, T. C.; Schmir, G. L. *J. Am. Chem. Soc.* **1959**, *81*, 4552.

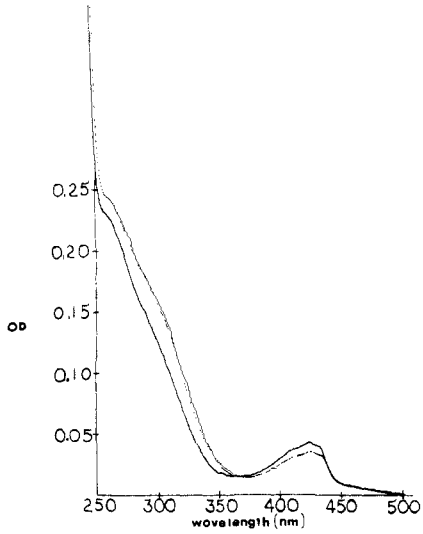

Figure 12. Spectrum of 1×10^{-5} M of $PPTH_{2T}$ (—) in pH 5.00, 1 M acetate buffer at 30 °C under anaerobic conditions. Spectrum (···) obtained for a solution of 1×10^{-5} M $PPTH_{2T}$ and 1×10^{-5} NMM under the above conditions.

total buffer concentration but by a lesser amount. Thus, the species which decomposes to PPT_{ox} during the second phase are formed in a buffer-catalyzed non-rate-determining step. This observation and the rate law for the second phase strongly suggest that this species is the C(4a)-adduct. The N(1)-adduct is reasonably proposed to form in competition with the C(4a)-adduct by a non-buffer-catalyzed process. As a result, the A/B ratio is observed to decrease with the total buffer concentration (loc. cit., Figure 4). The competing processes giving rise to the A/B ratio are depicted in eq 11. Since only ratios were obtained in this

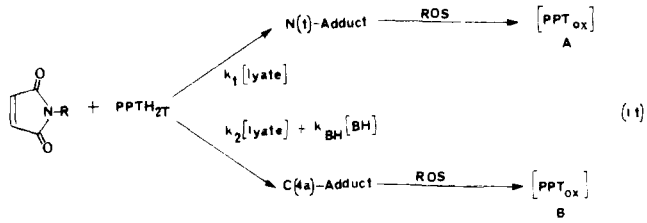

(11)

study, mechanistic details pertaining to the lyate and buffer species involved in these processes could not be assessed. We presume general acids are involved based on precedents.[2]

Aside from the C(4a)-adduct, the N(1)-adduct is the only other species possessing a single acid dissociation that could arise from the reaction of NMM and MI with $PPTH_{2T}$. Based on the high A/B ratio at most pH values, the N(1)-adduct predominates. Consistent with this assessment, the UV–visible spectrum obtained by mixing equal concentrations of $PPTH_{2T}$ and NMM (1×10^{-5} M) in anaerobic pH 5.00, 1 M acetate buffer largely resembles that of 1×10^{-5} M $PPTH_{2T}$ in the same buffer, Figure 12. The expected spectrum of the N(1)-adduct is based on our previous studies of $PPTH_{2T}$-mediated reduction of formaldehyde,[7b] where it was shown that N(1)- and N(5)-hydroxymethyl adducts possess UV–visible spectra nearly identical with authentic $PPTH_{2T}$. However, the adduct spectrum found in Figure 12 also possesses a shoulder at ~325 nm not found in $PPTH_{2T}$. This feature is ascribed to the presence of the C(4a)-adduct. Notably, the C(4a)-adduct in **2** (5-EtPPT-4a-OH) was observed to possess a λ_{max} value of 365 nm.[7b]

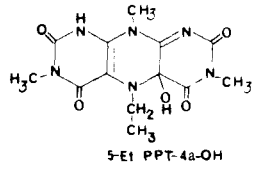

5-Et PPT-4a-OH

2

Table II. Second-Order Rate Constants for Hydroxide-Catalyzed C(4a)-Adduct Breakdown

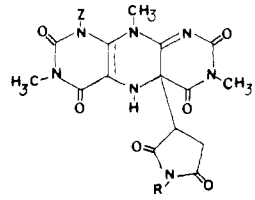

Z	R	k, M^{-1} s^{-1}
H	CH_3	6.35×10^6 (k_3)
(-)	CH_3	3.14×10^4 (k_4)
H	H	1.7×10^7 (k_3)
(-)	H	1.92×10^6 (k_4)

C(4a)-Adduct Breakdown. Decomposition of the C(4a)-adduct to PPT_{ox} and the reduced substrate follows the pH–rate law of eq 8. From eq 8, there may be seen to be two kinetically equivalent equations for the decomposition of the C(4a)-adduct to substituted succinimide and PPT_{ox} (eq 12 and 13). These expressions pertain

$$v = \left(\frac{kK_a}{a_H + K_a} + \frac{k_4K_w}{a_H}\right)[\text{C(4a)-adduct}_T] \quad (12)$$

$$v = \left\{\left(\frac{k_3a_H}{a_H + K_a}\right) + k_4\right\}\frac{K_w}{a_H}[\text{C(4a)-adduct}_T] \quad (13)$$

to spontaneous and hydroxide-catalyzed decomposition of the C(4a)-adduct anion (eq 12) and hydroxide-catalyzed decomposition of both the neutral C(4a)-adduct and its anion (eq 13). Since the C(4a)-maleimide adducts of lumiflavin are subject to hydroxide-catalyzed decomposition, the latter mechanism appears to be more reasonable.

The mechanism of hydroxide-catalyzed C(4a)-adduct decomposition is found in eq 14. That hydroxide catalysis involves a general rather than a specific base mechanism is supported by the following consideration. Specific base (equilibrium) formation

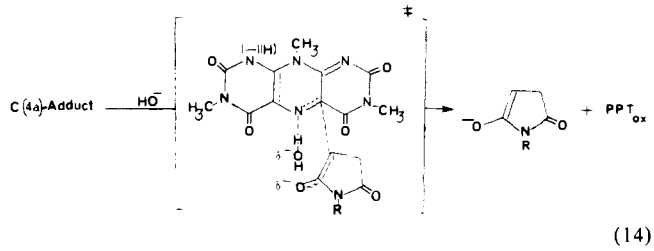

(14)

of the N(5)-anion ($pK_a > 20$) would require that the first-order rate constant for the elimination exceed the vibrational frequency of a bond at 30 °C [$k(s^{-1}) > kT/h = 6 \times 10^{12}$ s^{-1})]. Since buffer species employed to hold pH were not found in the rate law for C(4a)-adduct breakdown (loc. cit.), the conclusion is made that the transition state in eq 14 is late with regard to proton transfer. In this situation, the Brønsted β value would approach 1 and the C(4a)-adduct would exhibit a high selectivity toward hydroxide.[10] The general base catalyzed mechanism of eq 14 thus envisions N(5)-proton removal in concert with departure of the anionic product.

The second-order rate constants for hydroxide-catalyzed C(4a)-adduct decomposition calculated from fits of kinetic data by eq 13 are found in Table II. The second-order rate constants are 2.27×10^4 and 8×10^3 M^{-1} s^{-1} for hydroxide-catalyzed breakdown of the respective neutral NMM and MI C(4a)-adducts of lumiflavin (FlH_2).[2] Comparison of these constants with those for breakdown of neutral NMM and MI C(4a)-adducts of $PPTH_2$

(10) Bell, A. R. P. "The Proton in Chemistry", 2nd Ed. Cornell University Press: New York, 1973.

(Table II) reveal that a 280–2100-fold rate increase accompanies the change of reductant from lumiflavin (FlH_2) to the pyrimido[5,4-g]pteridine system ($PPTH_2$). These enhancements are seen as a consequence of the lower reduction potential of $PPT_{ox} \rightarrow PPT^{2-}$ ($E^{\circ\prime} = -0.346$ V) compared to $Fl_{ox} \rightarrow Fl$ ($E^{\circ\prime} = -0.198$ V).[7] Thus, the driving force for the PPT_{ox} formation is much greater than that for Fl_{ox} formation. The relative rates mentioned above are also reflected in the acid-catalyzed reduction of formaldehyde to methanol by PPT^{2-} (3.3×10^6 M^{-2} s^{-1}) and by Fl^- (2.3×10^4 M^{-2} s^{-1}).[7b,11] The presence of an anion delocalized in the fused pyrimidine ring of the MI and NMM C(4a)-adduct [Z = (–), R = CH_3 and H in Table II] results in a 10–200-fold decrease, respectively, in the second-order rate constant compared to that for the neutral C(4a)-adducts. These rate decreases likely result from higher pK_a values for N(5)-proton dissociation in the anionic species.

The fitting of log (k'_{obsd}) vs. pH data for C(4a)-adduct breakdown (Figures 5B and 9B) to eq 13 provides the kinetic dissociation constants $pK_a = 3.96$ and 3.37. The pK_a values are taken as the acid dissociation constants from the respective neutral NMM and MI C(4a)-adducts of $PPTH_{2T}$. The lower values, compared to acid dissociation from $PPTH_2$ ($pK_a = 5.51$), likely result from the loss of the central 8π-electron dihydropyrazine ring upon C(4a)-adduct formation. The presence of this electron-rich antiaromatic ring system[12] is expected to destabilize the anion in the fused pyrimidine ring of $PPTH^-$ compared to the C(4a)-adduct anion. Consistent with this assessment, the N(1)-adduct of NMM and MI has the central dihydropyrazine ring intact and the N(9)-proton dissociates with pK_a values of 6.65 and 6.72, respectively.

N(1)-Adduct Breakdown. The fate of the NMM and MI N(1)-adducts of $PPTH_{2T}$ is discussed in conjunction with Scheme I. In Scheme I, with either substrate, formation of the anionic N(1)-adduct is followed by its conversion to an N(1),N(9)-diadduct in a rapid equilibrium step. The N(9),C(4a)-diadduct is then formed off this equilibrium from the anionic N(1)-adduct in a slow irreversible step. In non-rate-determining steps, the N(9),C(4a)-diadduct undergoes base-catalyzed elimination of the anionic reduced substrate followed by elimination of NMM or MI from the N(9)-position to provide PPT_{ox}.

This mechanism is seen as consistent with the lumiflavin-mediated reductions of NMM and MI studied previously[2] as well as the findings of this study which indicate that product formation must occur via C(4a)-adducts. Thus, plots of k_{obsd} vs. substrate concentration possess a zero intercept which inidcates that the N(1)-adduct itself is not forming PPT_{ox} (Figures 2 and 3). Since the N(1)-adduct does not form PPT_{ox}, neither should the N(1),N(9)-diadduct. The formation of N(5)-maleimide adducts of FlH_{2T} has not been observed, and thus we dismiss the formation of an N(1),N(5)-diadduct. Venkataram and Bruice[2] have concluded that C(4a)-adduct formation from FlH^- is general acid catalyzed. Likewise, the rate-determining formation of the C(4a)-adduct from the N(1)-adduct during the first phase of PPT_{ox} formation involves the anionic form of the N(1)-adduct (Figures 5A and 9A) and is buffer-catalyzed (Figures 3 and 7). Buffer catalysis, however, is important only at high acidity. Found in eq 15 is the proposed mechanism for C(4a)-adduct formation which assumes general-acid catalysis by buffer acids and lyate species.

It was noted that the N(1)-adduct forms in competition with the formation of the C(4a)-adduct (loc. cit.). Thus, it is reasonable to assume that the formation of the N(1),N(9)- and N(9),C(4a)-diadducts occurs from the N(1)-adduct. The N(1),N(9)-diadduct is expected to be unstable as a result of steric interactions with the N(10)-methyl group. We postulate that this diadduct is in a rapid equilibrium with the N(1)-adduct. Saturation in MI, seen below pH 5.0, during the first phase of the reactions (Figures

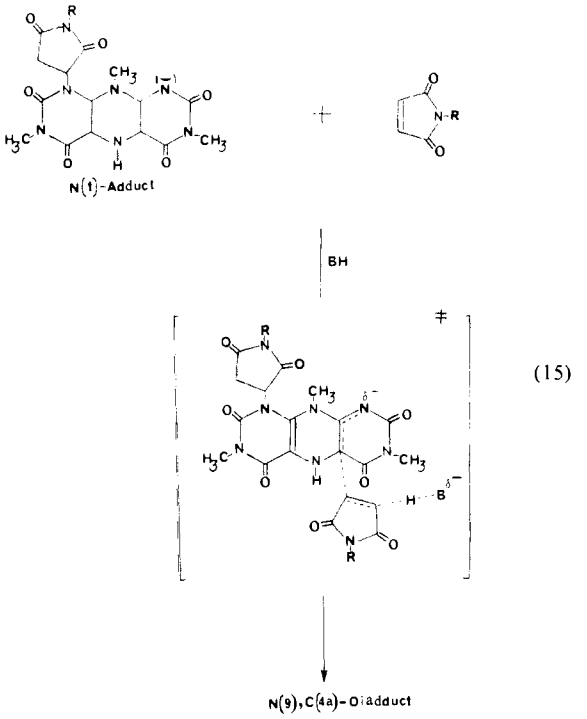

(15)

6 and 7) is likely associated with the accumulation of the N(1),N(9)-diadduct. At all pH values and concentrations studied, there could be found no evidence of saturation in NMM. There would seem to be little doubt, however, that the mechanisms for reductions of NMM and MI are identical and that saturation in NMM would be seen at higher concentrations. Because of the facility of reduction, reactions could not be studied at higher [NMM] values.

Equation 16 pertains to the kinetics of reduction of NMM and MI during phase 1. In eq 16, [S] = [NMM] or [MI] and k_5, K, and K_{a2} are the constants found in Scheme I. Under the

$$v = \frac{k_5 K_{a2}[S]}{a_H + K_{a2}(1 + K[S])}[\text{N(1)-adduct}_T] \qquad (16)$$

nonsaturating conditions of $K[S] \ll 1$, eq 16 becomes eq 17. It is seen that eq 17 possesses the same form as the empirical rate law found in eq 7 which was employed to fit log k_{lyate} (M^{-1} s^{-1}) vs. pH data for the first phase of PPT_{ox} formation (Figures 5a and 9a). Thus, $\bar{k}$ in eq 7 is the second-order rate constant (k_5

$$v = \frac{k_5 K_{a2}}{a_H + K_{a2}}[S][\text{N(1)-adduct}_T] \qquad (17)$$

in Scheme I) for C(4a)-adduct formation from the N(1)-adduct anion. The calculated values of k_5 for NMM and MI are 125 and 58.5 M^{-1} s^{-1}, respectively.

In a non-rate-determining step, the N(9),C(4a)-diadduct is proposed to undergo hydroxide-catalyzed elimination of the succinamide anion at k_6 (M^{-1} s^{-1}). The estimated value of k_6 is 1×10^7 M^{-1} s^{-1} based on second-order rate constants for hydroxide-catalyzed breakdown of the neutral C(4a)-adducts found in Table II. The pseudo-first-order rate constant for N(9),C(4a)-diadduct breakdown at pH 7.00 would then be 1.48 s^{-1}, a value much greater than the k_{obsd} values measured for C(4a)-adduct formation at this pH (0.02–0.12 s^{-1}) under pseudo-first-order conditions in NMM (Figure 2). The rate of formation of C(4a)-adducts when starting with FlH_{2T} and $PPTH_{2T}$ is faster than the like rate when starting with the N(1)-adducts of $PPTH_2$. The change in the rate-determining step from the C(4a)-adduct breakdown to the C(4a)-adduct formation when starting with the N(1)-adduct of $PPTH_2$ likely results from (1) the lower nucleophilicity of the N(1)-adduct anion compared to PPT^{2-} as a consequence of one less negative charge and (2) the formation of a neutral N(9),C(4a)-diadduct which is 200 times (Table II) more

(11) (a) Williams, R. F.; Bruice, T. C. *J. Am. Chem. Soc.* **1976**, *98*, 7752. (b) Williams, R. F.; Shinkai, S. S.; Bruice, T. C. *Ibid.* **1977**, *99*, 921.

(12) (a) Bruice, T. C.; Yano, Y. *J. Am. Chem. Soc.* **1975**, *97*, 5263. (b) Hemmerich, P.; Jorns, M. S. "Enzymes, Structure and Function"; Dreuth, G., Oosterbaan, R. A., Veeger, C., Eds.; Elsevier: Amsterdam, 1972; p 95.

Scheme II

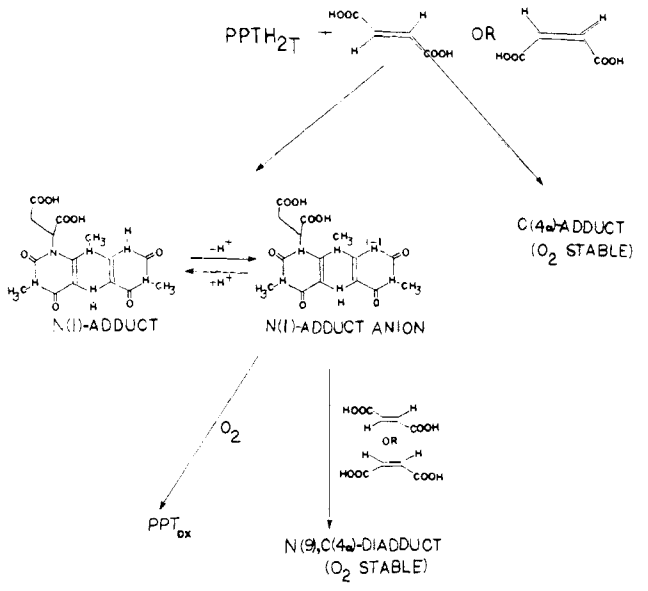

susceptible to hydroxide attack than the anionic C(4a)-adduct formed from PPT^{2-}.

The reduction of fumaric and maleic acids derivatives by $PPTH_{2T}$ likely follows the same mechanism (Scheme I) proposed for $PPTH_{2T}$ reduction of NMM and MI. Thus, the evidence cited indicates the formation of C(4a)-adducts which are refractive to oxidation by oxygen but which in time slowly form PPT_{ox} and the reduced substrate.

The reactions of fumaric and maleic acids with $PPTH_{2T}$ are quite slow so that only initial rates have been followed. The slow reactions observed could pertain to either the rapid formation of adducts which slowly form products or rate-determining formation of adducts on the pathway to products. Support for the former alternative derives from the kinetics of aerobic reoxidation of reaction mixtures studied at various reaction times and substrate concentrations (loc. cit., Results section). As depicted in Scheme II, $PPTH_{2T}$ reacts with fumaric and maleic acids to form a mixture of N(1)- and C(4a)-monoadducts. Reaction mixtures held at pH 4.00 and incubated for only 1×10^4 s likely consist of nearly equal amounts of these adducts. This assessment is based on the ratios of N(1)- to C(4a)-monoadducts observed in the $PPTH_{2T}$-mediated reduction of NMM at this pH value (Figure 4B). Admittance of air at 1×10^4 s results in the slow oxidation of the N(1)-adduct to PPT_{ox} (41–45%). The C(4a)-adduct, on the other hand, is not air-oxidized,[2] resulting in the low yield of PPT_{ox}. Longer incubation times apparently result in conversion of the N(1)-adduct to the N(9),C(4a)-diadduct as in Schemes I and II. Thus, reaction mixtures (pH 4.00) incubated for a longer period of time than 2×10^4 s prior to oxygen admittance provide less PPT_{ox} product. Reactions carried out at pH 7.00 likely provide mostly the N(1)-adduct which rapidly reoxidizes to PPT_{ox} upon admittance of air. At this pH, the yield of PPT_{ox} obtained on O_2 oxidation is independent of the incubated time and concentration of substrate. The predominance of the N(1)-adduct at pH 7.00 is predicted from the high N(1)- to C(4a)-adduct ratios observed at this pH value for $PPTH_{2T}$-mediated reduction of NMM, Figure 4A. The greater rate of oxidation of N(1)-adducts of $PPTH_{2T}$ at pH 7.00 as compared to pH 4.00 is due to the dissociation of the N(1)-proton (pK_a of 6.65 for N(1)-NMM adduct of $PPTH_2$), Scheme II.

In contrast to the reductions of maleic acid fumaric acids, the reductions of their mono- and diethyl esters proceed by a first-order rate law to afford PPT_{ox} in 75–100% yield. The mechanisms of the $PPTH_{2T}$-mediated reduction of fumaric and maleic acids and their esters are proposed to be the same. The difference in reactivity of esters and acids is best explained by the facility of the elimination reactions associated with k_3, k_4, and k_6 of Scheme I. In these reactions, the C(4a)-adducts decompose to form PPT_{ox} and the anion of the reduced substrate. When maleic and fumaric acids are substrates, there is required to be eliminated the α-carbanion of dissociated succinic acid. The lessened resonance stabilization of the carboxylate carbanion, as compared to the like carbanion of the esters, should greatly impede the elimination reaction in the case of acid substrates. Reactions associated with k_3 and k_4 are rate limiting for all substrates examined. It is reasonable to suppose that with NMM, MI, and the fumaric and succinic esters, $k_5 + k_{BH}[BH]$ also represent rate-limiting steps and that for the succinic and fumaric acids substrates, $k_6[HO^-]$ becomes a rate-limiting step. The phenomena of saturation by carboxylate ester substrates is attributed to, as in the case of NMM and MI, the accumulation of an N(1),N(9)-diadduct.

Acknowledgment. This work was supported by a grant to T.C.B. from the National Science Foundation and a grant to E.B.S. from The National Cancer Institute, PHS No. 1 R01 CA 36876-01.

Registry No. MI, 541-59-3; NMM, 930-88-1; $PPTH_2$, 82639-48-3; PPT(ox), 82639-46-1; C(4a)-(NMM)$PPTH_2$, 100113-43-7; C(4a)-(NMM)$PPT_{(ox)}$, 100113-43-7; C(4a)-(MI)$PPTH_2$, 100113-45-9; C(4a)-(MI)$PPT_{(ox)}$, 100113-46-0; N(a)-C(4a)-$(MI)_2PPTH_2$, 100113-47-1; N(a)-C(4a)-$(NMM)_2PPTH_2$, 100113-48-2; N(1)-(maleic acid adduct)($PPT_{(ox)}$), 100113-49-3; N(a)-C(4a)-(maleic acid diadduct)-$(PPTH)_2$, 100113-50-6; ethyl fumarate, 2459-05-4; diethyl fumarate, 623-91-6; diethyl maleate, 141-05-9; fumaric acid, 110-17-8; maleic acid, 110-16-7; *N*-methylsuccinimide, 1121-07-9; diethyl succinate, 123-25-1.